Z. Phys. C – Particles and Fields 9, 67–80 (1981)

Zeitschrift für Physik C Particles and Fields

Inclusive γ-Decays of Heavy 1^{--} Quarkonium: Rates, Spectra, Angular Correlations and Photon Polarizations

J. G. Körner

Deutsches Electronen-Synchrotron DESY, D-2000 Hamburg, Federal Republic of Germany

D. W. McKay*

II. Institut für Theoretische Physik der Universität, D-2000 Hamburg, Federal Republic of Germany

Received 17 December 1980

Abstract. We present detailed results on the calculation of the decay of a heavy 1^{--} quarkonium state into a photon and two vector gluons in Born approximation. We tabulate and graph the formulas for the Dalitz plots, the photon energy spectrum, the angular correlations between the γ-event plane and the beam direction, and for the linear polarization asymmetry of the produced photon. We compare the QCD results with a model where the heavy 1^{--} quarkonium state decays into a photon and two colored, scalar gluons.

I. Introduction

The γ-inclusive decays of heavy $J^{PC}=1^{--}$ quarkonium states constitute an important test of perturbative QCD (quantum chromodynamics), which predicts that these decays proceed by $1\gamma+2$ gluon emission [1–3]. DORIS data [4] already support the QCD 3-gluon origin of the purely hadronic decays of Υ (9.46), and PETRA data [5, 6] at higher energies beautifully confirm the QCD predictions on the $q+\bar{q}+$gluon origin of hadronic jets. The γ-inclusive decays of 1^{--} charmonium states are quite a clean and independent check of the QCD theory.

Measurement of inclusive, direct photon decays of the J/ψ show roughly the rate expected in QCD [7, 8]. In one experiment [7], the photon spectrum is much softer than that expected from the QCD calculation. The second experiment [8] shows a harder spectrum, not inconsistent with QCD. Apart from the experimental discrepancy, the relatively low energy per decay-gluon which is available at the J/ψ mass makes suspect the application of perturbative QCD to the decay of J/ψ. The structure observed in $J/\psi\to\gamma+X$ and $\psi'\to\gamma+X$ [9] gamma-energy spectra also indicate that the Born term cannot be the whole story in the J/ψ region. Since one expects the perturbative QCD predictions to be more reliable at higher gluon energies, the prospects of significant increases in Υ-data from CESR and DORIS and possibly VEPP 4 in the next few years encourage us to review and extend the calculations of γ-inclusive decays of quarkonium [1–3]. The disadvantage in rate of γ-inclusive decays (the branching ratio should be roughly 1/4 that of the corresponding ψ/J inclusive-γ branching ratio, or about 2%) is compensated for by the obvious advantage that the photon's energy and direction can be measured and directly be used in the analysis of the process. The corresponding analysis of the three gluon process will always involve uncertainties related to the non-perturbative fragmentation process of the gluons.

Since the quarkonium is produced in a polarized state in e^+e^- interactions, there will be correlations between the decay plane and the beam axis which provide important tests of the dynamics of the decay process. The well-defined orientation of the γ-inclusive event allows one to measure and test these correlation predictions. For the purely hadronic decay of Υ, the polar correlation has already been measured, and it is consistent with the QCD Born approximation prediction [10]. Since the $\gamma+2$ gluon process is everywhere infrared finite, the four correlation coefficients calculated via QCD turn out to be of roughly the same magnitude in this process as expected, and beam-event correlations are correspondingly strong.

Photon polarization measurements, should they prove feasible, would enlarge the number of testable coefficients. Just the total polarization asymmetry measurement would yield valuable information about the mechanism which underlies quarkonium decay.

In the derivation of cross-sections and correlation coefficients, we use the helicity formalism throughout. This method has considerable technical advantage in these calculations. Since its application to quarkonium decay is new, we exhibit some intermediate steps.

* Alexander von Humbolt fellow on leave from the University of Kansas, Lawrence, Kansas, USA

0170-9739/81/0009/0067/$02.80

Results for colored, scalar gluon amplitudes are also derived in every case, and several comparisons with QCD are made.

In the next section we write down the matrix elements for the vector case and give helicity amplitudes and the helicity structure functions (cross-sections) $\sigma_U, \sigma_L, \sigma_T$, and σ_I which appear in the rate formula. Differential and integrated rates are given. In Sect. 3 we present our results for the rates, spectra, integrated helicity structure functions, average opening angle between gluon jets, polar angle distributions, average thrust and polarization asymmetries. An appendix contains the outline of the helicity formalism applied to the scalar gluon case, and detailed formulas are tabulated there and referred to in the figures and remarks in the main text.

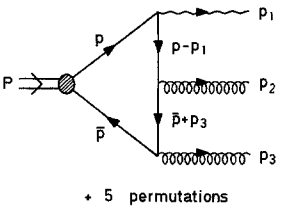

Fig. 1. The basic Feynman graph for the process: quarkonium $\to g+g+\gamma$ considered in this paper. p_1 always represents the photon momentum

II. Matrix Elements and Helicity Amplitudes

The calculation of the decay of a heavy quarkonium state into a photon and two vector gluons proceeds in complete analogy to the corresponding positronium decay calculation. Figure 1 illustrates the process. In the nonrelativistic approximation, and neglecting binding energies, one has $M \cong 2m$ and $P = p - \bar{p} \cong 2p$, where M and m are the masses of the quarkonium state and its heavy quark constituent, respectively. For the spin projection of the quarkonium state, it is convenient to use the covariant form $\not{\epsilon}(P-M) = 2\not{\epsilon}(\not{p}-m)$, which is well known from relativistic $SU(6)$ calculations [11]. The amplitude is then given by the covariant trace

$$M_{ij} = N_{ij}\{2m\,\mathrm{Tr}[\not{\epsilon}(\not{p}-m)\not{\epsilon}_3^*(-\not{p}+\not{p}_3-m)^{-1}\not{\epsilon}_2^*(\not{p}-\not{p}_1-m)^{-1}\not{\epsilon}_1^*] + \text{cyclic perm. } (1,2,3)\}. \tag{1}$$

All constants have been absorbed into $N_{ij} = N\delta_{ij}$, where i,j are color indices and

$$N = 2\sqrt{2}\,\sqrt{\alpha}\,\alpha_s(4\pi)^{3/2} e_Q \psi(o)/(\sqrt{3}\,m^{3/2}).$$

$\psi(o)$ is the wave function evaluated at the origin, e_Q is the charge of the heavy quark, and α and α_s are the electromagnetic and strong coupling constants, respectively. Decay rates are computed according to the rules for a massive spin one boson decaying into three massless bosons with the normalization indicated above.

After performing the trace calculation, the amplitude (1) can be arranged into the convenient form [12]

We have used the conventional scaled energies $x_i = E_i/m$, so that $x_1 + x_2 + x_3 = 2$. Useful formulas are: $P \cdot p_i = m^2 x_i$, $p_i \cdot p_j = 2m^2(1-x_k)$ where $i \neq j \neq k$, and $(P-p_i)^2 - m^2 = 2m^2 x_i$ which occur in the propagator denominators.

In the usual approach, cross sections are derived from (2) by squaring and summing over spins. We shall instead calculate helicity amplitudes first and then obtain cross sections by evaluating the appropriate sums of bilinear forms of helicity amplitudes. One can extract all needed physics information directly from the bilinears of helicity amplitudes, which have simple forms. This procedure is shorter and more transparent than the usual one of squaring and summing on spins – especially in the cases where polarization projections are necessary.

Our event coordinate system is fixed according to Fig. 2. The z-direction points along the photon momentum and the x-axis is in the half plane of the higher momentum gluon. Momenta are $p_1 = E_1(1;001)$, $p_2 = E_2(1; \sin\theta_{12}, 0, \cos\theta_{12})$, $p_3 = E_3(1; -\sin\theta_{13}, 0, \cos\theta_{13})$ and polarization vectors are (1 = photon and 2, 3 = gluons)

$$e_1^{*\pm} = \frac{1}{\sqrt{2}}(0; \pm 1, -i, 0), \qquad e_2^{*\pm} = \frac{1}{\sqrt{2}}(0; \cos\theta_{12}, -i, \mp\sin\theta_{12})$$

$$e_3^{*\pm} = \frac{1}{\sqrt{2}}(0; \pm\cos\theta_{13}, -i, \pm\sin\theta_{13}),$$

$$e^{\pm} = \mp\frac{1}{\sqrt{2}}(0; 1, \pm i, 0) \quad \text{and} \quad e^0 = (0; 0, 0, 1).$$

$$\begin{aligned} M_{ij} = -2N_{ij}\frac{m^{-4}}{x_1 x_2 x_3}\{&(e_1^* \cdot e_2^*)[-(p_1 \cdot p_3)(p_2 \cdot e_3^*)(p_1 \cdot e) - (p_1 \cdot p_3)(p_2 \cdot p_3)(e_3^* \cdot e) - (p_2 \cdot p_3)(p_1 \cdot e_3^*)(p_2 \cdot e)] \\ &+ (e \cdot e_3^*)[(p_1 \cdot p_3)(p_2 \cdot e_1^*)(p_3 \cdot e_2^*) - (p_1 \cdot p_2)(p_3 \cdot e_1^*)(p_3 \cdot e_2^*) + (p_2 \cdot p_3)(p_1 \cdot e_2^*)(p_3 \cdot e_1^*)] \\ &+ (1 \leftrightarrow 3) + (2 \leftrightarrow 3)\}. \end{aligned} \tag{2}$$

Here θ_{ij} is the angle between particles i and j. From spin counting, one finds that there are twelve independent helicity amplitudes, designated $H_{\lambda_1\lambda_2\lambda_3;\lambda_{Q\bar{Q}}}$ as follows:

Transverse $Q\bar{Q}$ polarization

$$H_{+++;+}=0$$
$$H_{++-;+}=(1-x_2)(1-x_3)$$
$$H_{+-+;+}=(1-x_2)(1-x_3)$$
$$H_{+--;+}=(1-x_1)x_1^2$$
$$\otimes\text{common}\ \frac{1}{2}N_{ij}\cdot\frac{1}{x_1^2x_2x_3}\ \text{factor} \quad (3a)$$
$$H_{-++;+}=0$$
$$H_{-+-;+}=(1-x_1)(1-x_2)^2$$
$$H_{--+;+}=(1-x_1)(1-x_3)^2$$
$$H_{---;+}=0.$$

Longitudinal $Q\bar{Q}$ polarization

$$H_{+++;0}=0$$
$$H_{++-;0}=\sqrt{2}(1-x_3)X^{1/2}$$
$$\otimes\text{common}\ \frac{1}{2}N_{ij}\cdot\frac{1}{x_1^2x_2x_3}$$
$$H_{+-+;0}=-\sqrt{2}(1-x_2)X^{1/2}$$
$$H_{+--;0}=0$$

where $X=(1-x_1)(1-x_2)(1-x_3)$.

The remaining twelve helicity amplitudes can be obtained from the parity conditions

$$H_{-\lambda_1,-\lambda_2,-\lambda_3;-}=H_{\lambda_1,\lambda_2,\lambda_3;+}$$
$$H_{-\lambda_1,-\lambda_2,-\lambda_3;0}=-H_{\lambda_1,\lambda_2,\lambda_3;0}. \quad (3b)$$

Since the initial spin-one quarkonium is produced in a polarized state in e^+e^--annihilation, beam-event correlations allow one to measure four decay structure functions, also loosely referred to as cross-sections, which are denoted by σ_U, σ_L, σ_T, and σ_I. The distribution is written as*

$$\frac{d\Gamma}{dx_1\,dx_2\,d\chi\,d\cos\theta}=\frac{\mathrm{m}}{8(4\pi)^4}[\sigma_U(1+\cos^2\theta)+2\sigma_L\sin^2\theta$$
$$+2\sigma_T\sin^2\theta\cos2\chi-2\sqrt{2}\sigma_I\sin2\theta\cos\chi]. \quad (4)$$

The polar angle θ and azimuthal angle χ are defined as drawn in Fig. 2. Measurements of σ_U, σ_L, and σ_T do not require energy ordering of the two gluons, but *only require that the event plane be determined.* Measurement of σ_I requires that gluon jet energies be measured and ordered. The reason for this difference between measurement of σ_I and measurement of σ_U, σ_L or σ_T is seen as follows. When, as in QCD, the particles 2 and 3 are identical, then the coefficients σ_U, σ_L, and σ_T are symmetric in exchange of x_2 and x_3. σ_I is antisymmetric in x_2 and x_3. For an arbitrary χ value, the first three terms in (4) obtain equal contributions from points (x_2, x_3) and points (x_3, x_2), whereas the last term obtains cancelling contributions. But if the choice of χ is correlated with the energy identification (x-axis as in Fig. 2 in the half plane of the more energetic jet), then the $\cos\chi$ coefficient always has the same sign, and a non-trivial distribution results.

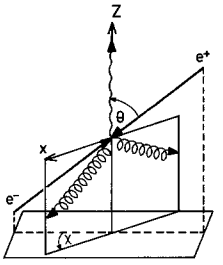

Fig. 2. The event coordinate system which we use to define angular correlations. When energy ordering is required, the x-axis is taken to be in the half-plane of the more energetic gluon

Now the four cross-sections in (4) can be expressed in terms of the helicity amplitudes of (3) by the relations

$$\sigma_U=2\sum_{\lambda_i}|H_{\lambda_1\lambda_2\lambda_3;+}|^2$$
$$\sigma_L=\sum_{\lambda_i}|H_{\lambda_1\lambda_2\lambda_3,0}|^2$$
$$\sigma_T=\mathrm{Re}\sum_{\lambda_i}H_{\lambda_1\lambda_2\lambda_3;+}H^*_{\lambda_1\lambda_2\lambda_3;-} \quad (5)$$
$$\sigma_I=\mathrm{Re}\sum_{\lambda_i}H_{\lambda_1\lambda_2\lambda_3,+}H^*_{\lambda_i\lambda_2\lambda_3;0},$$

where color summing has not been explicitly displayed in (5).

Since σ_I does require energy ordering $x_2>x_3$ in its measurement, we assume energy ordering to be done in the whole differential rate (4) and therefore include no 1/2 factor appropriate to identical gluons when all of phase space is integrated over. As remarked above, energy ordering is not necessary for σ_U, σ_L, and σ_T which are correspondingly $x_2\leftrightarrow x_3$ symmetric, as seen in Table 1.

Armed with expressions (3) and (5), it is now an easy matter to calculate the cross-sections σ_U, σ_L, σ_T, and σ_I. We display these double differential quantities, which should be designated, e.g., $\sigma_U(x_1, x_2)$, in Table 1. The results agree with those of Koller and Walsh and of Koller et al. [2].

* The extension of (4) to include transverse beam polarization effects is straightforward (see [2])

Table 1. The double differential decay cross-sections when polarization of the photon is not detected – QCD predictions. The arguments x_i of the σ_i are suppressed for convenience. $X \equiv (1-x_1)(1-x_2)(1-x_3)$ and $N_{ij}^2 \equiv N^2 \delta_{ij} \delta_{ij} = 8N^2$

$$\sigma \equiv \sigma_U + \sigma_L = \frac{2N_{ij}^2}{x_1^2 x_2^2 x_3^2} \cdot [x_1^2(1-x_1)^2 + x_2^2(1-x_2)^2 + x_3^2(1-x_3)^2]$$

$$\sigma_L \equiv \sigma_L^{\parallel} + \sigma_L^{\perp} = \frac{4N_{ij}^2}{x_1^4 x_2^2 x_3^2} [(1-x_2)^2 + (1-x_3)^2] \cdot X$$

$$\sigma_T \equiv \sigma_T^{\parallel} + \sigma_T^{\perp} = \frac{1}{2} \sigma_L$$

$$\sigma_I \equiv \sigma_I^{\parallel} + \sigma_I^{\perp} = \frac{N_{ij}^2 \sqrt{2X}}{x_1^4 x_2^2 x_3^2} \{(1-x_2)(1-x_3)(x_2-x_3) + (1-x_1)[(1-x_2)^3 - (1-x_3)^3]\}$$

Table 2. Difference between double differential in- and out-of-plane polarized photon cross-sections in QCD case

$$\sigma^- \equiv \sigma^{\parallel} - \sigma^{\perp} = -\frac{4N_{ij}^2}{x_1^2 x_2^2 x_3^2} \cdot X$$

$$\sigma_L^- \equiv \sigma_L^{\parallel} - \sigma_L^{\perp} = -\frac{8N_{ij}^2}{x_1^4 x_2^2 x_3^2} \cdot X \cdot (1-x_2)(1-x_3)$$

$$\sigma_T^- \equiv \sigma_T^{\parallel} - \sigma_T^{\perp} = -\frac{2N_{ij}^2}{x_1^4 x_2^2 x_3^2} \cdot (1-x_2)^2 (1-x_3)^2 [1 + (1-x_1)^2]$$

$$\sigma_I^- \equiv \sigma_I^{\parallel} - \sigma_I^{\perp} = \frac{\sqrt{2} N_{ij}^2}{x_1^4 x_2^2 x_3^2} \cdot X^{1/2} \cdot (1-x_2)(1-x_3)(x_2-x_3)(2-x_1)$$

We have listed the total differential decay cross-section $\sigma = \sigma_U + \sigma_L$ in Table 1 instead of σ_U, since σ takes the simple form which is well known from the positronium calculation of Ore and Powell [13]. Note that σ_T and σ_I need not be positive definite since they are interference terms.

The cross-sections σ_i in Table 1 correspond to measurements where the polarization of the photon goes undetected, i.e. they are the sum $\sigma_i^{\parallel} + \sigma_i^{\perp}$, where $\sigma_i^{\parallel}$ and $\sigma_i^{\perp}$ are the corresponding rates with the photon being linearly polarized parallel and perpendicular, respectively, to the three-body event plane. The degree of linear polarization of the produced photon is given by the polarization asymmetry $A = (\sigma^{\parallel} - \sigma^{\perp})/(\sigma^{\parallel} + \sigma^{\perp})$. These quantities can also be calculated easily from the helicity amplitudes. One has

$$\sigma_U^{\parallel} - \sigma_U^{\perp} = -4 \sum_{\lambda} \mathrm{Re}[(H_{+\lambda_2 \lambda_3; +})(H^*_{-\lambda_2 \lambda_3; +})]$$

$$\sigma_L^{\parallel} - \sigma_L^{\perp} = -2 \sum_{\lambda} (H_{+\lambda_2 \lambda_3; 0})(H^*_{-\lambda_2 \lambda_3; 0})$$

$$\sigma_T^{\parallel} - \sigma_T^{\perp} = -\sum_{\lambda} [(H_{+\lambda_2 \lambda_3; +})(H^*_{-\lambda_2 \lambda_3; -}) + (H_{+\lambda_2 \lambda_3; -})(H^*_{-\lambda_2 \lambda_3; +})]$$

$$\sigma_I^{\parallel} - \sigma_I^{\perp} = -\sum_{\lambda} \mathrm{Re}[(H_{+\lambda_2 \lambda_3; +})(H^*_{-\lambda_2 \lambda_3; 0}) + (H_{+\lambda_2 \lambda_3; 0})(H^*_{-\lambda_2 \lambda_3; +})].$$

The differential distribution for the cross section difference in- and out-of-the production plane is the same as given in (4). In Appendix B we discuss an additional independent polarization contribution due to linear polarization in the $x = y$ plane. This additional contribution does not, however, enter into the polar angle polarization distributions considered in this paper.

In the following we shall sometimes use the abbreviations $\sigma_i^{\pm} = \sigma_i^{\parallel} \pm \sigma_i^{\perp}$ where $\sigma_i^{+} \equiv \sigma_i$. The QCD expressions for these photon polarization-sensitive quantities are shown in Table 2, where again the x_1 and x_2 arguments of the σ_i are suppressed. The scalar gluon model predictions for the eight observables listed in Tables 1 and 2 are presented in the appendix.

III. Results

In this section we accumulate results of our calculations. We discuss in turn the expected rates of charmonium decay to γgg compared to ggg in the vector and scalar gluon cases, the Dalitz plots and photon energy spectra which one expects, the polar beam-event correlation coefficient $\alpha(x_1)$, the average cosine of the opening angle between gluons, and the photon polarization asymmetry as it varies within the Dalitz plot boundaries, as it varies as a function of the photon momentum alone, and as it varies with photon angle. In addition, average gluon thrust is computed as a function of x_1, and also averaged over x_1.

(a) Rates

The lowest order QCD rate prediction is quite simple [1, 2] and is obtained by comparing the graph of Fig. 1 with the corresponding one where the photon is replaced by a gluon. One finds

$$R_\gamma = \frac{\Gamma(Q\bar{Q} \to \gamma gg)}{\Gamma(Q\bar{Q} \to ggg)} = \frac{36}{5} \frac{\alpha}{\alpha_s} e_Q^2, \tag{6}$$

where α ist the electromagnetic fine-structure constant and α_s ist the corresponding strong interaction constant and where e_Q is the quark charge in units of e. The Lena collaboration at DESY [14] quotes a value $\alpha_s(M_\Upsilon^2)=0.16^{+0.04}_{-0.02}\pm 0.01$ from their analysis of Υ total width and leptonic branching ratios. With a b-quark charge of $e_Q=-1/3$, one estimates

$$R_\gamma \cong 0.038^{-0.009}_{+0.005}. \tag{7}$$

The corresponding ratio in the scalar gluon case is complicated by the presence of infrared singularities. These singularities result from taking the quarks real rather than virtual and neglecting binding of quarks within the quarkonium [15].

The perturbative on-mass-shell treatment of the decay process will therefore be no longer reliable for small gluon energies. One must therefore introduce a cut-off on the gluon energy which may be reasonably estimated to be of the order of the binding energy in the quarkonium state. We quote the value of the ratio R_γ as a function of the cutoff,

$$R_\gamma = \frac{16}{3}\frac{\alpha}{\bar{\alpha}_s}(e_Q)^2 \cdot \frac{I^{gg\gamma}(\Delta)}{I^{ggg}(\Delta)} = \frac{e_Q^2}{\bar{\alpha}_s}\cdot(0.39)\frac{I^{gg\gamma}(\Delta)}{I^{ggg}(\Delta)}, \tag{8}$$

where $\bar{\alpha}_s$ is the scalar gluon coupling constant, the functions $I^{gg\gamma}(\Delta)$ and $I^{ggg}(\Delta)$ are defined in (A.4) and (A.5) of the appendix. The range of the final, divergent x_1 integration is cut off at $x=\Delta$ below and $1-\Delta$ above, since the ggg amplitude blows up in the $x\to 0$ and $x\to 1$ limits. Taking several cut-off values we find

$$\begin{aligned} I^{gg\gamma}/I^{ggg} &= 1.00 \quad \Delta = 0.0 \\ I^{gg\gamma}/I^{ggg} &= 1.42 \quad \Delta = 0.01 \\ I^{gg\gamma}/I^{ggg} &= 2.09 \quad \Delta = 0.05 \\ I^{gg\gamma}/I^{ggg} &= 2.28 \quad \Delta = 0.10 \\ I^{gg\gamma}/I^{ggg} &= 2.38 \quad \Delta = 0.20, \end{aligned} \tag{9}$$

for a variation of about a factor two over these Δ values. For a rough estimate, this cutoff dependence poses no problem. As examples, we take the value $I^{gg\gamma}/I^{ggg}=2.28$ at $\Delta=0.10$, and we take two different values of $\bar{\alpha}_s$ which have been quoted in recent experimental analyses. The (bad) fit value $\bar{\alpha}_s=0.77$ by the PLUTO group [16] gives $R_\gamma \cong 0.08$, which is about twice as large as the estimate, (7), for the vector gluon case*. The TASSO value [17] $\bar{\alpha}_s=1.6$ (also poor confidence level) leads to $R_\gamma \cong 0.04$.

* Recent PLUTO data rules out a scalar gluon description of $\Upsilon\to$hadrons [10]

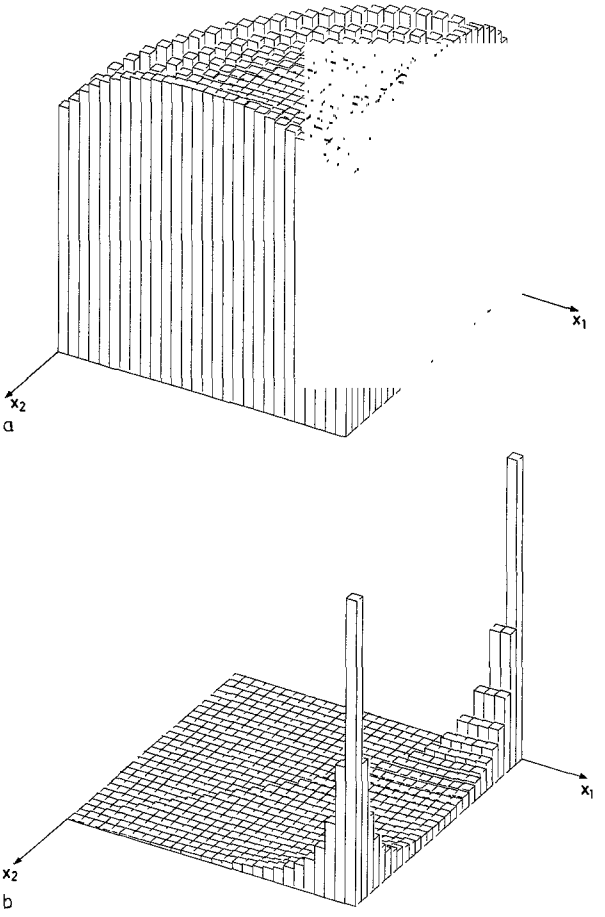

Fig. 3a and b. Dalitz plot distribution for $gg\gamma$ final state **a** vector gluons **b** scalar gluons

(b) Dalitz Plot Distributions and Energy Spectra

Turning next to the question of the spectra of the final state in γgg decay of quarkonium, we show the double differential decay rate summed over all spins in Fig. 3a. The formula is listed in Table 1. The distribution has the rather uniform appearance already displayed by Koller and Walsh [2] for $gg\gamma$ and for the ggg case of a totally hadronic final state. The corresponding scalar gluon distribution is shown in Fig. 3b for comparison, and the strong spin dependence is immediately obvious. The scalar distribution formula is listed in the appendix, Table 5.

The remarks of Walsh and Zerwas [19] and Koller and Krasemann [18] concerning the three gluon case are appropriate here. They pointed out that the soft scalar gluon region is infrared singular because of the lack of spin-flip suppression of the pole in the quark propagator in the limit of a zero momentum gluon. As discussed above, the singularity is a theoretical artifact, a result of treating the quarks as on shell. The binding energy provides a very rough estimate of how far off

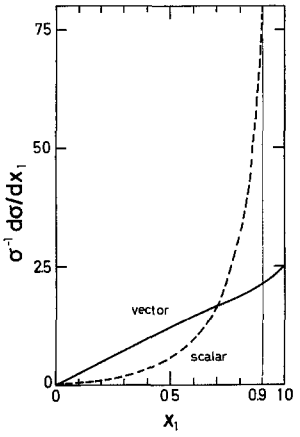

Fig. 4. The photon energy spectra in the QCD case (solid line) and scalar case (dashed line). Both curves are normalized to 1 in the interval [0, 0.9] for purposes of comparison

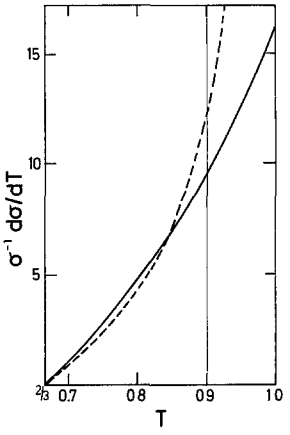

Fig. 5. Thrust distribution. Normalization as in Fig. 4

shell the bound quark is, though the ratio of $gg\gamma$ and ggg rate is not very sensitive to the precise value as indicated in our discussion in connection with (8) and (9). We choose $x=0.9$, or $\Delta=0.1$, as a cutoff in normalizing and displaying spectra in the photon energy variable, x_1. As in the case of three gluon final states [18, 19], the enhancement of decay probability when one scalar gluon is soft leads to an event configuration which is more like two jets than like three jets. The photon recoils against one gluon, the other gluon playing little role.

This two-jet-like feature of the scalar case is shown in another way by the comparison of the QCD x_1-spectrum and the scalar gluon spectrum in Fig. 4. The scalar spectrum is very hard, rising sharply above the QCD spectrum at an x_1 value of about 0.7. The spectra shown are both normalized to 1 in the interval [0, 0.9]. The QCD spectrum is almost linear in x_1 (as in a $\gamma+2$ jets phase space model), deviating slightly from linearity near $x_1=1$. In Fig. 5 we show the corresponding thrust distributions, normalized to 1 in the thrust interval [2/3, 0.9]. Again the QCD case shows an almost linear dependence on thrust, whereas the scalar gluon case has the more peaked behaviour characteristic of the infrared singularity as $T\to 1$.

The beam-event correlation (4), when summed over photon and gluon spins and integrated over gluon energies, contains the four independent cross-sections, or structure functions, shown in Table 3 for the QCD case and in Table 6 of the appendix for the scalar case. These cross-sections are plotted in Fig. 6a and b, respectively.

One notes from Fig. 6a that the helicity cross-sections for the QCD-case are of comparable magnitude, whereas for scalar gluons σ_U dominates over σ_L, σ_T, and σ_I over most of the x_1-range. The dominance of σ_U in the scalar gluon case results from its infrared singular nature as $x_1\to 1$, just as in the QCD $q\bar{q}g$ situation [10]. The QCD results, shown in Fig. 6a, encourage one to expect that the correlation cross-sections σ_U, σ_T, and σ_L can be individually measured, since photon momentum and the event plane are the only essential information needed.

(c) The Polar Correlation Parameter

In Fig. 7 is shown a plot of the value of α, the photon angular distribution parameter, as a function of x_1, the

Table 3. Single differential cross-sections where the photon polarization goes undetected – QCD case. The argument x_1 of the σ_i is suppressed, where x_1 is the scaled photon energy

$$\sigma \equiv \sigma^{\parallel}+\sigma^{\perp}=\frac{2N_{ij}^2(1-x_1)}{x_1(2-x_1)^3}\left\{\frac{(2-x_1)^4}{1-x_1}+x_1^2(2-x_1)+2[(2-x_1)^3-(1-x_1)x_1^2]\frac{\ln(1-x_1)}{x_1}\right\}$$

$$\sigma_L \equiv \sigma_L^{\parallel}+\sigma_L^{\perp}=-\frac{2N_{ij}^2(1-x_1)}{x_1(2-x_1)^3}\left\{(2-x_1)\left[2+6\frac{(1-x_1)}{x_1^2}\right]+\left[6(1-x_1)+x_1^2+12\frac{(1-x_1)^2}{x_1^2}\right]\frac{\ln(1-x_1)}{x_1}\right\}$$

$$=\sigma_L^{-}-\sigma^{-} \text{ (see Table 4)}$$

$$\sigma_T \equiv \sigma_T^{\parallel}+\sigma_T^{\perp}=\frac{1}{2}\sigma_L$$

$$\sigma_I \equiv \sigma_I^{\parallel}+\sigma_I^{\perp}=\frac{N_{ij}^2\sqrt{2}\sqrt{1-x_1}}{(2-x_1)x_1^3}\left[(2-x_1)^2+\frac{2(1-x_1)}{2-x_1}(2-x_1+x_1^2)-\sqrt{1-x_1}(2-x_1)(6-3x_1+x_1^2)\frac{\arcsin\left(\frac{x_1}{2-x_1}\right)}{x_1}\right]$$

scaled photon energy [2]. α measures the decay of quarkonium into $\gamma+$ two gluons as a function of the angle between the photon direction and the e^+e^- beam direction,

$$d\sigma/d\cos\theta \sim 1+\alpha\cos^2\theta$$

where

$$\alpha=(\sigma_U-2\sigma_L)/(\sigma_U+2\sigma_L)$$

and σ_U and σ_L are proportional to the probabilities that the decaying quarkonium state is transversely or longitudinally polarized in the photon direction, respectively. QCD predicts a distinctively sharp variation in the region $0.5 \leqq x_1 \leqq 1$ which should be testable and is certainly distinct from the scalar gluon case for which α is essentially 1 over the whole range due to the dominance of σ_U.

That $\alpha \to 1$ as $x_1 \to 1$ in both cases follows from the spin constraints on back-to-back particles with $J=1$ whose s_z projection along their colinear line of motion is necessarily ± 1. The distribution for decay of a state with $J=1$ and $J_{z'}=\pm 1$ ($z'=$ beam direction) into a state with $J=1$ and $J_z=\pm 1$ along a new z direction at angle θ with respect to z' (z is the photon direction), is just $1+\cos^2\theta$, or $\alpha=1$ and $\sigma_L=0$.

Choosing the z-axis along the photon's momentum is particularly well suited for seeing the distinctive QCD behavior in the polar angle distribution as compared to the scalar gluon case. If one uses the normal to the event plane to analyze the polar angle distributions, one obtains almost identical, flat distributions in both cases. To see this, transform the helicity cross-sections to a system where the normal to the event plane is the z-axis (transversity frame). One has in the new system [2]

$$\begin{aligned}\hat{\sigma}_U &= \tfrac{1}{2}\sigma_U+\sigma_L-\sigma_T \\ \hat{\sigma}_L &= \tfrac{1}{2}\sigma_U+\sigma_T\end{aligned} \tag{10}$$

and consequently

$$\begin{aligned}\hat{\alpha} &= (\hat{\sigma}_U-2\hat{\sigma}_L)/(\hat{\sigma}_U+2\hat{\sigma}_L) \\ &= -\tfrac{1}{3}(\sigma_U-2\sigma_L+6\sigma_T)/(\sigma_U+\tfrac{2}{3}\sigma_L+\tfrac{2}{3}\sigma_T).\end{aligned}$$

For QCD one has $\hat{\alpha}=-1/3$ since $\sigma_L=2\sigma_T$ (Table 1) and thus no x_1-dependence of $\hat{\alpha}$. For scalar gluons one finds again $\hat{\alpha}\cong -1/3$ for $x_1 \to 1$ due to the dominance of σ_U in the infrared limit. For smaller x_1-values, $\hat{\alpha}$ will become more negative. For example, one has $\hat{\alpha}(0) = -0.60$ and $\hat{\alpha}(0.5)=-0.47$.

In Fig. 8a we have plotted the QCD average values of α, polarization asymmetry A and "grand average" thrust $\langle\langle T\rangle\rangle$, where the averages are taken in the interval $[x_1^c, 1]$. In Fig. 8b we have plotted the corresponding averages taken in the interval $[x_1^c, 0.9]$ for

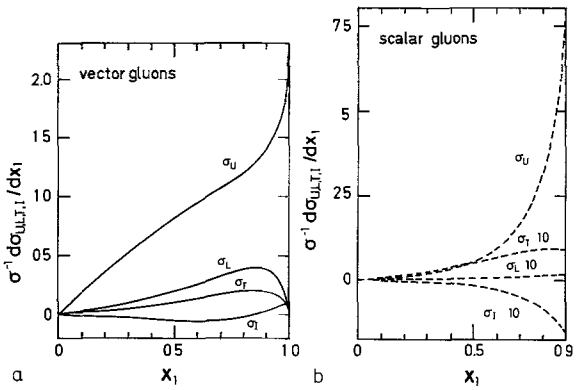

Fig. 6a and b. Beam-event correlation cross-sections σ_U, σ_L, σ_T, and σ_I as a function of photon energy. **a** Vector gluons. $\sigma=\sigma_U+\sigma_L$ normalized to 1 in [0, 1]. **b** Scalar gluons. $\sigma=\sigma_U+\sigma_L$ normalized to 1 in [0, 0.9]

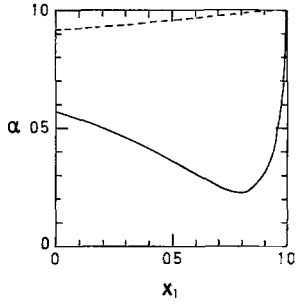

Fig. 7. The photon polar angle distribution coefficient, α, as a function of photon energy in the QCD case (solid line) and scalar model (dashed line)

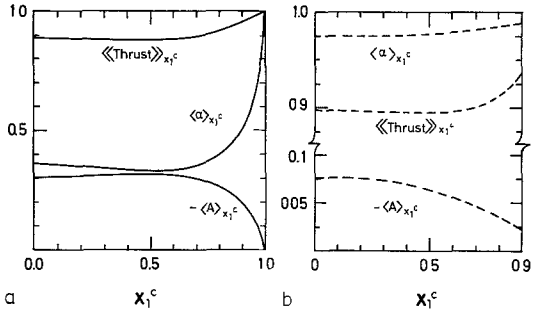

Fig. 8a and b. $\langle\alpha\rangle$, $\langle\langle$thrust$\rangle\rangle$ and $\langle A\rangle$ as functions of x_1^c; **a** vector case and **b** scalar case

the scalar gluon case. We have displayed the dependence of the averages on the lower cutoff x_1^c because low momentum photons are difficult to distinguish from background experimentally, and experimental data will generally only be available above some $x_1^c > 0$ which depends on the particular detector. Published data are limited to $x_1^c \gtrsim 0.5$, [8, 9] for example.

We avoided $x_1=1$ in the scalar gluon case because the infrared singularity in the model calculation at $x_1=1$ drives the averages to their value at $x_1=1$, for

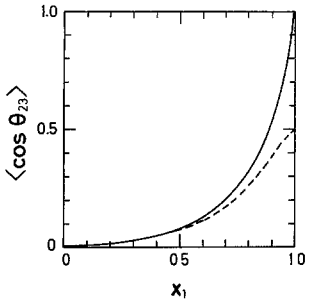

Fig. 9. $\langle\cos\theta_{23}\rangle$ vs. x_1

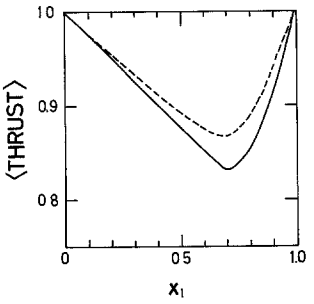

Fig. 10. ⟨thrust⟩ as function of x_1

example $\langle\alpha\rangle=\alpha(1)=1$, regardless of the lower integration limit x_1^c. Thus we define

$$\langle\alpha\rangle\equiv\frac{\int_{x_1^c}^{x_1^u}\alpha(x_1)\sigma(x_1)\,dx_1}{\int_{x_1^c}^{x_1^u}\sigma(x_1)\,dx_1}$$

and where $x_1^u=1$ or 0.9 for QCD or scalar gluons, respectively. The plots show vividly that there is a big difference between the scalar gluon model predictions and those of QCD for the energy-averaged photon angular correlation. This difference persists in every averaging range except for x_1^c very close to 1.

We continue our discussion by turning to the predictions for the average of the cosine of the opening angle between gluons and then return to Fig. 8a, b for remarks on "grand average" thrust and average polarization asymmetry.

(d) Average Opening Angle

In the average opening angle between the gluon jets $\langle\cos\theta_{23}\rangle$, an interesting difference between the vector gluon case and the scalar gluon case developes as $x_1\to 1$. $\langle\cos\theta_{23}\rangle$ is shown in Fig. 9, where one sees the expected back-to-back gluon configuration, $\langle\cos\theta_{23}\rangle\simeq -1$, for small photon momentum in both the scalar and vector gluon cases. But the singularity in the cross-section for the scalar case in the $x_1\to 1$ limit gives such strong weight to the emission of a soft gluon, whose direction is unconstrained while the other gluon recoils against the photon, that the opening angle *averages* to $\pi/2$. The vector case behaves normally, and the gluons must be parallel as they recoil against the photon in the $x_1\to 1$ limit where the photon has half the decay energy. The QCD $\langle\cos\theta_{23}\rangle$ behavior is, in fact, practically indistinguishable from the phase space prediction.

(e) Average Thrust

Υ decay into hadrons produces events which are more planar than the background events [4]. There is an associated decrease in thrust on the Υ resonance compared to the thrust of $e^+e^-\to$ hadron events off the Υ resonance [4]. This evidence supports the QCD picture that the final state in Υ decay originates from 3 gluons. A well defined event plane is necessary for extracting azimuthal and polarization dependence in quarkonium decay into $\gamma+$ hadrons, and we plot the average thrust in Fig. 10 as a function of x_1 to indicate the degree of expected planarity. Average thrust is defined as

$$\langle T(x_1)\rangle=\frac{\int T\sigma(x_2)\,dx_2}{\int\sigma\,dx_2},$$

where $T=x_1$, x_2 or x_3, depending on which is largest. The integration limits of the numerator depend upon whether x_1 is the largest, intermediate, or smallest energy. For each x_1 value, the integration region has two parts corresponding to the possibilities $x_2>x_3$ or $x_3>x_2$. The QCD prediction is seen to lie below the scalar model prediction at every x_1-value – another demonstration of the two-jet-like aspect of the scalar case. The QCD curve, incidentally, is almost identical to phase space, as was the case in $\langle\cos\theta_{23}\rangle$ discussed above.

The average of $\langle T\rangle$ over various x_1 regions – "grand average" thrust $\langle\langle T\rangle\rangle$ – is shown as a function of x_1^c in Fig. 8a. For example, if the data is averaged over the photon energy interval $0.5\leqq x_1\leqq 1$, QCD predicts that $\langle\langle T\rangle\rangle=0.82$, where

$$\langle\langle T\rangle\rangle\equiv\frac{\int_{x_1^c}^{1}\langle T\rangle\sigma\,dx_1}{\int_{x_1^c}^{1}\sigma\,dx_1}.$$

The corresponding plot in the scalar gluon case is shown in Fig. 8b.

(f) Polarization Asymmetry

So far we have only discussed measurements where the photon polarization is not detected. In order to extract the photon-polarization dependent observables $\sigma_{||}(x_1)$ and $\sigma_{\perp}(x_1)$, a polarization sensitive measurement must be made, and the asymmetry $A=(\sigma_{||}-\sigma_{\perp})/(\sigma_{||}+\sigma_{\perp})$ is the most accessible to direct measurement. To measure A, one must measure the difference between the number of events with linear photon polarization in the event plane and the number of events with linear photon polarization perpendicular to the event plane.

In Fig. 11a we show the variation of the asymmetry parameter over the Dalitz plot in the case of the QCD prediction, and in Fig. 11b we show the corresponding plot in the case of the scalar gluon model prediction. The asymmetry is largest in the large x_1 region of the Dalitz plot in the QCD prediction. The scalar prediction is largest in the small x_1 region, giving a distribution which is easily distinguishable from that of QCD. For orientation we note that the maximum asymmetry in the QCD case occurs for values $x_1=x_2=x_3=2/3$, where $A=-0.5$, while the maximum occurs in the scalar case for values $x_1=0$, $x_2=x_3=1$ where $A=-0.6$. We note that the QCD asymmetry distribution plotted in Fig. 11a is in agreement with that of Brodsky et al. [3].

The quantities $\sigma_{||}-\sigma_{\perp}$, Table 2, are integrated over the gluon energies and presented as functions of x_1 in Table 4 for the QCD case and in the appendix for the scalar gluon case.

We plot next the asymmetry as a function of x_1 in Fig. 12, and the QCD and scalar gluon results are seen to be distinctively different. The remarkable fact is that *the asymmetry is large and negative*, 30%–40%, *over just the range* $0.5<x_1<0.9$ *of photon energies which is acceptable* (in both the general and technical senses) *experimentally*. In both cases the photon is polarized perpendicular to the event plane.

Comparing Figs. 11 and 12, one notes further that, since Fig. 12 represents an average over all gluon

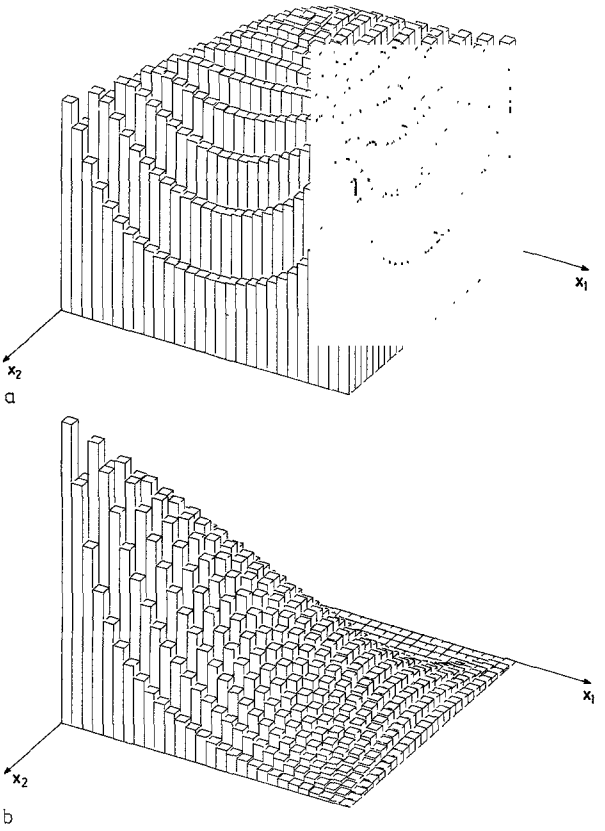

Fig. 11a and b. Dalitz plot distribution of polarization asymmetry **a** vector gluons **b** scalar gluons

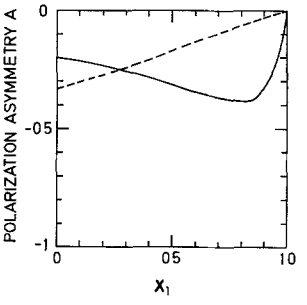

Fig. 12. The x_1-dependence of the polarization asymmetry in the QCD (solid line) and scalar (dashed) cases

Table 4. Differences between in- and out-of-plane polarized photon single differential cross-sections in QCD case

$$\sigma^{-}\equiv\sigma^{||}-\sigma^{\perp}=\frac{4N_{ij}^2(1-x_1)}{x_1(2-x_1)^3}\left\{2-x_1+(2-2x_1+x_1^2)\frac{\ln(1-x_1)}{x_1}\right\}$$

$$\sigma_L^{-}\equiv\sigma_L^{||}-\sigma_L^{\perp}=-\frac{4N_{ij}^2(1-x_1)}{x_1^3(2-x_1)^3}\left\{(2-x_1)(6-6x_1+x_1^2)+4(1-x_1)(3-3x_1+x_1^2)\frac{\ln(1-x_1)}{x_1}\right\}$$

$$\sigma_T^{-}\equiv\sigma_T^{||}-\sigma_T^{\perp}=\frac{[1+(1-x_1)^2]}{4(1-x_1)}\sigma_L^{-}$$

$$\sigma_I^{-}\equiv\sigma_I^{||}-\sigma_I^{\perp}=\frac{\sqrt{2}(2-x_1)\sqrt{1-x_1}}{x_1^3}\left\{\frac{2(1-x_1)}{(2-x_1)^2}+1-\frac{3(1-x_1)}{x_1\sqrt{1-x_1}}\arcsin\left(\frac{x_1}{2-x_1}\right)\right\}N_{ij}^2$$

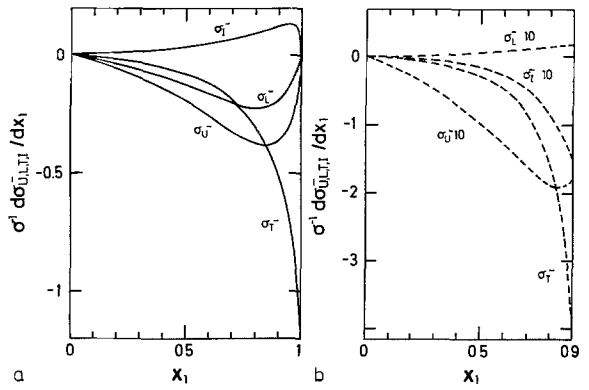

Fig. 13a and b. $\sigma_i^{\parallel} - \sigma_i^{\perp}$ as functions of x_1 **a** vector gluons, **b** scalar gluons. Normalization as in Fig. 6

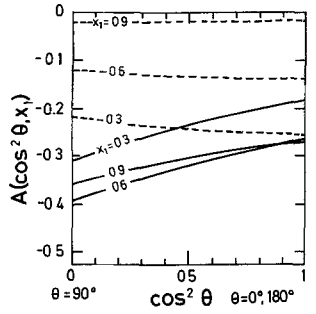

Fig. 14. The $\cos\theta$ dependence of the polarization asymmetry for various x_1 values

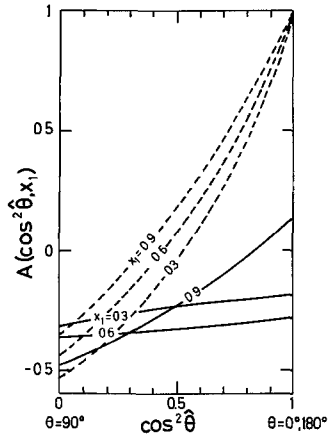

Fig. 15. The $\cos\hat{\theta}$ dependence of the polarization asymmetry. $\hat{\theta}$ is the angle between the normal to the event plane and the e^- beam direction

energies, there are regions of the Dalitz plot where the asymmetry is larger than 40%. One can tune the asymmetry optimally if events near the center of the Dalitz plot are selected. Whatever data sample one uses, the observation of a negative asymmetry in the $0.5 < x_1 < 1$ region would be strong support for the picture of quarkonium decay via the QCD mechanism shown in Fig. 1.

So far we have restricted ourselves to consideration of the total asymmetry, which is obtained by integrating over all angles [refer to (4)]. Angular dependence of the asymmetries is determined by σ_U^-, σ_L^-, σ_T^-, and σ_I^-, and we display these cross-sections as functions of x_1 in Fig. 13a, b for the QCD and scalar cases, respectively. In the scalar gluon model, σ_T^- is related to σ_U^+ by

$$\sigma_T^+ = -\tfrac{1}{2}\sigma_U^- \tag{11}$$

and it is clear that σ_T^- is the dominant asymmetry cross-section as $x_1 \to 1$. In the QCD case, $H_{++-;+}$ and $H_{+-+;+}$, (3a), are dominant as $x_1 \to 1$. All others have factors of $(1-x_1)$ and go to zero as $x_1 \to 1$. One sees that (11) holds in this $x_1 \to 1$ limit for QCD, and since σ_U^+ is large as $x_1 \to 1$ (Fig. 6a) then σ_T^- is also large and negative in this limit. The implications of the large σ_T^- values for the angular dependence of the asymmetry is discussed below.

Considering first the θ-dependence of the asymmetry, obtained by integrating over the azimuthal angle χ [see (4) and Fig. 2], we show the asymmetry as a function of $\cos\theta$ for several different values of the scaled photon energy, x_1, in Fig. 14. One sees that in the vector gluon case, where the asymmetry effect is predicted to be large for large x_1 values, the $\theta = \pi/2$ configuration is optimal, but not significantly larger than the average asymmetry from the experimental standpoint. In other words, the $\cos\theta$ plot shows that little sensitivity to the polarization resulting from dynamics is lost in the integration over θ angles. However, referring to Fig. 13 and (4), it is clear that the large σ_T^- values near $x_1 = 1$ will produce strong azimuthal correlations which get lost in the polar angle distribution, in which the χ-dependence is integrated out.

In order to extract the dependence on azimuth, we take an indirect route and use the relations (10) which relate the θ and $\hat{\theta}$ correlation cross-sections [2]. Taking the normal to the event plane as the z-axis we have then

$$A(\cos\hat{\theta}, x_1) = \frac{\hat{\sigma}_U^-(1+\cos^2\hat{\theta}) + 2\sigma_L^-(1-\cos^2\hat{\theta})}{\hat{\sigma}_U^+(1+\cos^2\hat{\theta}) + 2\hat{\sigma}_L^+(1-\cos^2\hat{\theta})}$$

and, using (10), obtain

$$A(\cos\hat{\theta}, x_1) = \frac{(\frac{3}{2}\sigma_U^- + \sigma_L^- + \sigma_T^-) + \cos^2\hat{\theta}(-\frac{1}{2}\sigma_U^- + \sigma_L^- - 3\sigma_T^-)}{(\frac{3}{2}\sigma_U^+ + \sigma_L^+ + \sigma_T^+) + \cos^2\hat{\theta}(-\frac{1}{2}\sigma_U^+ + \sigma_L^+ - 3\sigma_T^+)}. \tag{12}$$

The result is plotted vs. $\cos^2\hat{\theta}$ for several x_1 values in Fig. 15. We note that limiting cases (i) $\cos^2\hat{\theta} = 0$, $x_1 \to 1$ where $A \to -1/3$ for both scalar and QCD predictions since $\sigma_T^- = -\frac{1}{2}\sigma_U^+$ in this limit (11), and (ii) $\cos^2\hat{\theta} = 1$,

$x_1 \to 1$ where $A = -2\sigma_T^-/\sigma_U^+ \to 1$! The QCD $\cos^2\hat{\theta}$ distribution changes rapidly as $x_1 \to 1$ and is practically the same at $x_1 = 1$ as the $x_1 = 0.9$ curve of the scalar case in Fig. 15.

The polarization asymmetries are strong, even in average quantities, and afford a rich source of detailed information about the dynamics of quarkonium decay.

The photon polarization asymmetry can be measured either by Bethe-Heitler [20–23] or by Dalitz pair [24, 25] e^+e^- conversion. To get a rough idea of the strength of the correlation between the plane of the photon polarization and the plane of the converted e^+e^- pair (in plane/out of plane ratio), one can use the value of 4/3 estimated by Wick [22] in the Bethe-Heitler case to find that the observed asymmetry should be about 1/7 the photon polarization asymmetry. In the Dalitz pair case, one has an in plane/out of plane ratio of 1/3. This "anti-correlation" leads to an observed asymmetry which is opposite in sign to the virtual photon's asymmetry and 1/2 as large in magnitude. This stronger (anti) correlation in the Dalitz-pair conversion makes up some of the $O(\alpha)$ loss in event rate of this process relative to the Bethe-Heitler conversion. Both of these measurements will be difficult of course, since high energy photons produce e^+e^- pairs with small opening angles.

IV. Conclusions

The decay of quarkonium $J^P = 1^{--}$ offers a rich source of information on the dynamics of quark-gluon interactions, and we have extended the calculation of the $Q\bar{Q}(1^{--}) \to gg\gamma$ in both vector and scalar gluon models to include all of the decay structure function asymmetries. We found that the helicity formalism outlined in Sect. II simplifies such calculations greatly in comparison with the usual, basis-independent projection and tracing techniques.

The QCD predictions for the beam-event angular cross-sections showed that the beam-event angular correlation coefficients are comparable in magnitude and should be measurable in upcoming experiments. We placed strong emphasis on the polarization asymmetry calculation and its possible experimental measurement. The asymmetry was determined to be large over much of the Dalitz plot, Fig. 11a, and the asymmetry, which is negative, is plotted as a function of the photon energy x_1 and shows a maximum effect of $\approx 40\%$ in the experimentally accessible range, as seen in Figs. 12 and 14. The latter figure shows the asymmetry plotted vs. $\cos\theta$ for several different values of x_1. Because $\sigma_T^- \to -\frac{1}{2}\sigma_U^+$ as $x_1 \to 1$, and σ_U is large, one predicts especially large polarization asymmetry near $\chi = \frac{\pi}{2}$ (4). This χ-dependent effect is contained in $\hat{\theta}$ distributions, and we show this in Fig. 15 where $A \to 1$ as $\cos\hat{\theta}$, $x_1 \to 1$.

These effects and the comparison, Fig. 6a, of the various correlation cross-sections lead us to conclude that detailed tests of QCD in quarkonium photon + hadrons are possible experimentally. For low mass states, the clean perturbative picture which we have used will be complicated by final state interactions among hadrons, of course. Resonant states [9] and/or gluon-gluon interactions will modify the QCD predictions.

Regarding scalar gluons, we found that the singular soft gluon region dominates the final state so much that the events are primarily composed of a hard photon recoiling against one hard gluon. The transverse unpolarized cross-section σ_U, which has the singularity, dominates the other cross-sections so much that the angular correlation and asymmetry effects are washed out. Figures 4, 6b, 11b, and 12 illustrate this result. The average thrust, shown in Fig. 10, is clearly and measurably higher in the scalar than in the QCD case.

Finally, we remark that effects, expected to arise at high energy due to $Z^0 \leftrightarrow \gamma$ interference effects, and which should be taken into account in discussing $t\bar{t}$ decay, leave the polar ($\cos^2\theta$) distributions of the photon and its linear polarization unaffected. More complex density matrices resulting from beam polarization and/or inclusion of weak effects have been analysed by Körner and Schiller [26].

Acknowledgement. We would like to thank K. Koller, M. Krammer, G. Weber, G. Wolf, and Y. Zaitsev for some useful discussions.

Appendix A

The Scalar Gluon Case

The matrix element M_{ij} for $Q\bar{Q}(1^{--}) \to \gamma +$ two scalar gluons can be easily calculated from the Feynman diagram of Fig. 1. It results in the same covariant trace as in (1) with α_s replaced by the effective scalar coupling constant $\bar{\alpha}_s$ and the omission of the polarization vector terms $\not{e}_2^*$ and $\not{e}_3^*$. The effective fermion-scalar gluon coupling is defined by $\bar{g}_s \bar{\psi} \frac{\lambda^t}{2} \psi s^t$. The trace calculation yields

$$M_{ij} = -8N_{ij} \frac{1}{x_1 x_2 x_3} \Big\{ (1 - x_2 x_3) e \cdot e_1^* + \frac{1}{2m^2} [(1 - x_2)(p_1 \cdot e)(p_2 \cdot e_1^*) + x_1 (p_2 \cdot e)(p_2 \cdot e_1^*)] \Big\}, \quad \text{(A.1)}$$

where N_{ij} is a normalization factor defined after (1). The helicity amplitudes $H_{\lambda_\gamma;\lambda_{Q\bar{Q}}}$ are given by

$$H_{+;+} = -8N_{ij}\cdot\frac{1}{x_1^2x_2x_3}\cdot[x_1(1-x_2x_3)-X],$$

$$H_{-;+} = -8N_{ij}\cdot\frac{1}{x_1^2x_2x_3}\cdot X, \quad \text{and} \tag{A.2}$$

$$H_{+;0} = 4\sqrt{2}N_{ij}\cdot\frac{1}{x_1^2x_2x_3}\cdot X^{1/2}\cdot(x_2-x_3),$$

where $X\equiv(1-x_1)(1-x_2)(1-x_3)$. The parity conditions are

$$\begin{aligned} H_{-\lambda_\gamma;-} &= H_{+\lambda_\gamma;+} \\ H_{-\lambda_\gamma;0} &= -H_{\lambda_\gamma;0}. \end{aligned} \tag{A.3}$$

In Table 5 we list the expressions for the unpolarized photon cross-sections which appear in (4). Since there are only three independent helicity amplitudes and these are real in Born approximation, (A.2), there are clearly many relationships among the eight $\sigma_i^{\pm}$. We write, therefore, all of the σ_i^- in terms of σ_i^+ quantities in Table 6.

Because the photon spectrum is more readily measurable than the double Dalitz distributions, we show the expressions for cross-sections which result after integration over gluon variables in Table 7 in the unpolarized photon case. The integrated σ_i^- are related to the σ_i^+ in the same way as shown in Table 6.

As remarked in the text and as is evident in Figs. 3b and 4, the scalar gluon rate blows up at $x_1\to 1$ as $1/(x_1-1)$. To compute the total rate, we cut off the x_1 integration according to $\Delta\leqq x_1\leqq 1-\Delta$, the lower cut-off included for uniformity in comparing with the three gluon case, where one needs the lower cutoff. The cutoff dependent expression for the total rate as a function of cutoff, referred to as $I^{gg\gamma}(\Delta)$ in the text, is defined by [see also (4)]

$$\begin{aligned} \Gamma_{ij}^{gg\gamma} &= \frac{m}{6\pi^3}N_{ij}^2\Big\{\frac{1}{8}[\mathscr{L}_2(1-\Delta)-\mathscr{L}_2(-1+\Delta)+\mathscr{L}_2(-\Delta)-\mathscr{L}_2(\Delta)+\ln(1-\Delta)\ln(2-\Delta)] \\ &\quad +\ln\Delta\ln(1+\Delta)+\ln\Delta\Big[-2+\frac{3}{4}\frac{\Delta}{1+\Delta}+\frac{5}{4}\cdot\frac{\Delta}{(1+\Delta)^2}-\frac{9}{4}\frac{\Delta}{1-\Delta}\Big] \\ &\quad +\ln(1-\Delta)\Big[2-\frac{3}{4}\frac{(1-\Delta)}{2-\Delta}-\frac{5}{4}\frac{(1-\Delta)}{(2-\Delta)^2}+\frac{9}{4}\frac{(1-\Delta)}{\Delta}\Big]-\frac{5}{4}\cdot\frac{1}{1+\Delta}+\frac{5}{4}\cdot\frac{1}{2-\Delta}\Big\} \\ &\equiv \frac{m}{6\pi^3}N_{ij}^2 I^{gg\gamma}(\Delta), \end{aligned} \tag{A.4}$$

where Δ is the photon energy cutoff and $\mathscr{L}_2(x) = -\int_0^x \frac{\ln(1-x')\,dx'}{x'}$ is the dilogarithm function.

Since we are interested also in the branching ratio of the γ-inclusive decay involving scalar gluons, we briefly recapitulate the total rate calculation $Q\bar{Q}(1^{--})\to$ three scalar gluons [18]. On evaluation of the Feynman diagram Fig. 1 corresponding to the three gluon case, one has

$$\begin{aligned} M_{ijk} &= N_{ijk}\,\mathrm{Tr}\{2m[\not{e}(\not{p}-m)(-\not{p}+\not{p}_3-m)^{-1} \\ &\quad\cdot(\not{p}-\not{p}_1-m)^{-1}]+\text{cycl. perm}\} \\ &= N_{ijk}\frac{4}{m}\cdot\frac{1}{x_1x_2x_3}\cdot(-p_1\cdot e(x_2-x_3) \\ &\quad +p_2\cdot e(x_1-x_3)-p_3\cdot e(x_1-x_2)), \end{aligned}$$

where $N_{ijk}=\frac{1}{2}f_{ijk}\cdot 2\sqrt{2}(\bar{\alpha}_s 4\pi)^{3/2}\psi(0)/(m^{3/2}\sqrt{3})$. The helicity amplitudes are

$$H_+ = 4\sqrt{2}N_{ijk}\frac{\sqrt{X}}{x_1^2x_2x_3}(3x_1-2)$$

$$H_0 = 8N_{ijk}\cdot\frac{1}{x_1^2x_2x_3}\cdot(x_2-x_3)(2x_1-1)$$

Table 5. Unpolarized photon double differential cross-sections in the scalar gluon model. $X=(1-x_1)(1-x_2)(1-x_3)$. Refer to (4) for the interpretation of the σ_i. Note $\sigma=\sigma_U+\sigma_L$. The σ_i arguments x_1, x_2, and x_3 are suppressed for notational reasons

$\sigma^{\parallel}+\sigma^{\perp}=64N_{ij}^2\cdot\frac{1}{x_1^2x_2^2x_3^2}\cdot[2(1-x_2x_3)^2-3X]$
$\sigma_L^{\parallel}+\sigma_L^{\perp}=64N_{ij}^2\cdot\frac{1}{x_1^4x_2^2x_3^2}\cdot(x_2-x_3)^2\cdot X$
$\sigma_T^{\parallel}+\sigma_T^{\perp}=128N_{ij}^2\cdot\frac{1}{x_1^4x_2^2x_3^2}\cdot[1-x_2x_3-x_1(1-x_1)]\cdot X$
$\sigma_I^{\parallel}+\sigma_I^{\perp}=-32\sqrt{2}N_{ij}^2\cdot\frac{X^{1/2}}{x_1^4x_2^2x_3^2}\cdot[x_1(1-x_2x_3)-2X](x_2-x_3)$

Table 6. Differences between double differential in- and out-of-plane photon polarization cross-sections in the scalar gluon model

$\sigma^{\parallel}-\sigma^{\perp}=\sigma_L^{\parallel}+\sigma_L^{\perp}-2(\sigma_T^{\parallel}+\sigma_T^{\perp})$
$\sigma_L^{\parallel}-\sigma_L^{\perp}=\sigma_L^{\parallel}+\sigma_L^{\perp}$
$\sigma_T^{\parallel}-\sigma_T^{\perp}=-\frac{1}{2}(\sigma_U^{\parallel}+\sigma_U^{\perp})$
$\sigma_I^{\parallel}-\sigma_I^{\perp}=\sigma_I^{\parallel}+\sigma_I^{\perp}$

and the parity condition is $H_- = -H_+$. We shall only give the result for $\sigma = \sigma_U + \sigma_L$ for the total rate calculation, (4)

$$\sigma = 64 N_{ijk}^2 \cdot \frac{1}{x_1^2 x_2^2 x_3^2}[x_2 x_3(5-9x_1) - (4-10x_1+5x_1^2)],$$

where $N_{ijk}^2 = \frac{N^2}{4} f_{ijk} f_{ijk} = 6N^2$. Integration over x_2 and x_1 then yields the expression for the total rate, including a statistics factor 1/6,

$$\begin{aligned}\Gamma^{ggg}(\Delta) = \frac{m}{24\pi^3} N_{ijk}^2 \Big\{ & 3[-\mathscr{L}_2(1-\Delta) + \mathscr{L}_2(-1+\Delta) + \mathscr{L}_2(\Delta) - \mathscr{L}_2(-\Delta) + \ln(1-\Delta)\ln(2-\Delta)] \\ & - \ln\Delta \ln(1+\Delta) + \frac{4}{3}\ln(1-\Delta)\left[1 - \frac{3}{2}\frac{1}{\Delta} + \frac{3}{2-\Delta} - \frac{1}{(2-\Delta)^2}\right] \\ & + \frac{4}{3}\ln(\Delta)\left[-1 + \frac{3}{2}\frac{1}{1-\Delta} - \frac{3}{1+\Delta} + \frac{1}{(1+\Delta)^2}\right] + \frac{4}{3}\left(\frac{1}{1+\Delta} - \frac{1}{2-\Delta}\right)\Big\} \\ \equiv & \frac{m}{24\pi^3} N_{ijk}^2 I^{ggg}(\Delta). \end{aligned} \tag{A.5}$$

Appendix B

Linear Photon Polarization in the $x = y$ Plane

In general the (unnormalized) photon density matrix $\varrho_{\lambda\lambda'}$ will involve four independent components, viz.

$$\varrho_{\lambda\lambda'} = \tfrac{1}{2}(\sigma \mathbb{1} + \varrho_x \boldsymbol{\sigma}_x + \varrho_y \boldsymbol{\sigma}_y + \varrho_z \boldsymbol{\sigma}_z). \tag{B.1}$$

A circular polarization component ϱ_z will only be present when parity violating effects or longitudinal beam polarization effects are included [26]. The y-component corresponding to linear photon polarization in the $x = y$ plane has not been considered in the main text since it does not contribute to the polar distributions worked out in this paper. For the sake of completeness we will list the relevant y-components in this appendix.

The double differential density matrix distribution is given by [26]

$$\begin{aligned}\frac{d\varrho}{dx_1\, dx_2\, d\cos\theta\, d\chi} \sim & \frac{3}{8}(1+\cos^2\theta)\,(\sigma_U \mathbb{1} + \varrho_{Ux}\boldsymbol{\sigma}_x) \\ & + \frac{3}{4}\sin^2\theta(\sigma_L \mathbb{1} + \varrho_{Lx}\boldsymbol{\sigma}_x) + \frac{3}{4}\sin^2\theta\cos 2\chi(\sigma_T \mathbb{1} + \varrho_{Tx}\boldsymbol{\sigma}_x) \\ & - \frac{3}{4}\sin^2\theta\sin 2\chi\varrho_{4y}\boldsymbol{\sigma}_y + \frac{3}{2\sqrt{2}}\sin 2\theta\sin\chi\varrho_{5y}\boldsymbol{\sigma}_y \\ & - \frac{3}{2\sqrt{2}}\sin 2\theta\cos\chi(\sigma_I \mathbb{1} + \varrho_{Ix}\boldsymbol{\sigma}_x). \end{aligned} \tag{B.2}$$

One notes from (B.2) that the ϱ_y contribution drops out after χ-integration as stated above.

The y-components of the density matrix can be expressed in terms of the x-components given in Tables 2 and 6 with $\sigma^{\parallel} - \sigma^{\perp} = -\varrho_x$.

QCD:

$$\varrho_{4y} = \varrho_{Tx}[1-(1-x_1)^2]/[1+(1-x_1)^2]$$

$$\varrho_{5y} = \varrho_{Ix} x_1/(2-x_1).$$

Scalar Gluon:

$$\varrho_{4y} = \varrho_{Tx} \cdot (H_{+;+}^2 - H_{-;+}^2)/(H_{+;+}^2 + H_{-;+}^2)$$

$$\varrho_{5y} = \varrho_{Ix} \cdot (H_{+;+} + H_{-;+})/(H_{+;+} - H_{-;+}).$$

Table 7. Single differential cross-sections as a function of photon energy x_1 for unpolarized photons in the scalar model. The x_1 argument of σ_i is suppressed

$$\sigma^{\parallel} + \sigma^{\perp} = \frac{64 N_{ij}^2}{x_1(2-x_1)^2(1-x_1)} \cdot \left\{2 + 3(1-x_1)^2 + (1-x_1)(2-x_1)^2 + \frac{(1-x_1)^2}{2-x_1}[6 + 2x_1 + 3(2-x_1)^2]\frac{\ln(1-x_1)}{x_1}\right\}$$

$$\sigma_L^{\parallel} + \sigma_L^{\perp} = -\frac{64 N_{ij}^2 (1-x_1)}{x_1^3(2-x_1)}\left\{3(2-x_1) + [6(1-x_1) + x_1^2]\frac{\ln(1-x_1)}{x_1}\right\}$$

$$\sigma_T^{\parallel} + \sigma_T^{\perp} = \frac{-64 N_{ij}^2 (1-x_1)}{x_1^3}\left\{1 + 2\frac{(1-x_1+x_1^2)}{(2-x_1)^2} + \frac{2}{(2-x_1)}\left[1 + (1-x_1)^2 - \frac{2(1-x_1+x_1)^2(1-x_1)}{(2-x_1)^2}\right]\frac{\ln(1-x_1)}{x_1}\right\}$$

$$\sigma_I^{\parallel} + \sigma_I^{\perp} = \frac{32\sqrt{2} N_{ij}^2 (1-x_1)^{1/2}(2-x_1)}{x_1^3}\left\{1 + 2\frac{(2-3x_1+2x_1^2)}{(2-x_1)^3} - \frac{1}{(1-x_1)^{1/2}}\left[2(1-x_1) + \frac{(2-3x_1+2x_1^2)}{(2-x_1)}\right]\left[\arcsin\left(\frac{x_1}{2-x_1}\right)\right]\Big/ x_1\right\}$$

The effect of the γ-components can be judged by considering the general parametrization of the (normalized) density matrix of a linearly polarized photon:

$$\varrho = \tfrac{1}{2}(\mathbb{1} + P_{\text{lin}}(\cos 2\varphi \sigma_x + \sin 2\varphi \sigma_y)). \quad \text{(B.3)}$$

From (B.3) one concludes that the polarization plane has an angle $\varphi = \frac{1}{2}\text{arcctg}(\varrho_x/\varrho_y)$ relative to the decay plane and the degree of polarization in this plane is given by $P_{\text{lin}} = (\varrho_x^2 + \varrho_y^2)^{1/2}/\sigma$.

References

1. M.Chanowitz: Phys. Rev. D**12**, 912 (1975)
2. K.Koller, T.Walsh: Nucl. Phys. B**140**, 449 (1978). Three gluons are treated by K.Koller, H.Krasemann, T.Walsh: Z. Phys. C – Particles and Fields **1**, 71 (1979)
3. S.Brodsky, D.G.Coyne, T.A.DeGrand, R.R.Horgan: Phys. Lett. **70**B, 234 (1977); S.Brodsky, T.A.DeGrand, R.F. Schwitters: Phys. Lett. **79**B, 225 (1978)
4. Ch.Berger et al.: Phys. Lett. **82**B, 449 (1979)
5. JADE Collaboration, W.Bartel et al.: Phys. Lett. **91**B, 142 (1980)
   Mark-J Collaboration, D.P.Barber et al.: Phys. Rev. Lett. **43**, 830 (1979)
   PLUTO Collaboration, Ch.Berger et al.: Phys. Lett. **86**B, 418 (1979)
   TASSO Collaboration, R.Brandelik et al.: Phys. Lett. **86**B, 243 (1979)
6. TASSO Collaboration: Evidence for a spin 1 gluon in three jet events. DESY 80/80, August 1980
   PLUTO Collaboration: A study of multijet events in e^+e^- annihilation. DESY 80/93, Oct. 1980
7. G.S.Abrams et al.: Phys. Rev. Lett. **44**, 114 (1980). Also see G.J.Feldman: Proceedings of the XV Rencontre de Moriond, March 15–21, 1980 and SLAC-PUB-2510 (1980)
8. M.T.Ronan et al.: Phys. Rev. Lett. **44**, 367 (1980)
9. R.Partridge et al.: Phys. Rev. Lett. **45**, 1150 (1980)
10. PLUTO Collaboration: Topology of the Υ-decay. DESY 80/117, Dec. 1980
11. R.Delbourgo, A.Salam, J.Strathdee: Proc. Roy. Soc. A**278**, 146 (1965)
    B.Sakita, K.Wali: Phys. Rev. Lett. **14**, 404 (1965). For a quark model formulation see T.Gudehus, DESY Report 68/11 (1968) unpublished; Phys. Rev. **184**, 1788 (1969)
12. M.Krammer: Phys. Lett. **74**B, 361 (1978); F.A.Berends, G.J.Komen: Nucl. Phys. B**119**, 112 (1977)
13. A.Ore, J.L.Powell: Phys. Rev. **75**, 1696 (1949)
14. LENA Collaboration: Total width and leptonic branching ratio of the Υ (9.46). DESY 80/53, June 1980
15. M.Krammer, H.Krasemann: Proceedings of the XVIII Int. Univ. für Kernphysik, Schladming, Austria 1979
16. PLUTO Collaboration: Ref. 6
17. TASSO Collaboration: Ref. 6
18. K. Koller, H.Krasemann: Phys. Lett. **88**B, 119 (1979)
19. T.Walsh, P.Zerwas: Phys. Lett. **93**B, 53 (1980)
20. C.N.Yang: Phys. Rev. **77**, 722 (1950)
21. T.H.Berlin, L.Mandansky: Phys. Rev. **78**, 623 (1950)
22. G.C.Wick: Phys. Rev. **81**, 467 (1951)
23. H.Olsen, L.C.Maximon: Phys. Rev. **114**, 887 (1959); L.C.Maximon, H.Olsen: Phys. Rev. **126**, 310 (1962)
24. M.Kobayashi, K.Kondo: Nucl. Instrum. Methods **104**, 101 (1972); K.Kondo et al.: Nucl. Instrum. Methods **114**, 365 (1974)
25. H.Olsen: Phys. Rev. **131**, 406 (1963); A.P.Potylitsyn: J. Nucl. Phys. **3**, 721 (1978)
26. J.Körner, D.Schiller: DESY Preprint (1981)

Note added in proof: In [26] the linear polarization of the produced photon has been analyzed in terms of components relative to the photon-beam plane. A polarization measurement of this component has the advantage that no reference need to be made to the hadronic part of the γ-inclusive event.